Proceedings of Meetings on Acoustics

Volume 21, 2014 http://acousticalsociety.org/

167th Meeting of the Acoustical Society of America
Providence, Rhode Island
5 - 9 May 2014

Session 3aUWb: Underwater Acoustics

Laboratory measurements of high-frequency, broadband acoustic scattering of growing sea ice and oil beneath sea ice

Christopher Bassett*, Andone Lavery, Ted Maksym and Jeremy P. Wilkinson

***Corresponding author's address: Department of Applied Ocean Physics and Engineering, Woods Hole Oceanographic Institution, Woods Hole, Massachusetts 02543, cbassett@whoi.edu**

The morphology of sea ice during the early stages of growth is strongly dependent on environmental conditions. Under calm conditions, congelation ice forms through downward growth of ice crystals from the water surface. Under turbulent conditions (surface waves), rapid freezing of ice crystals occurs in the upper water column (frazil ice), eventually consolidating into pancake ice through repeated collisions and agglomeration of the loose frazil crystals. It is expected that high-frequency scattering from the basal layer of the ice varies for different sea ice types and can reveal structural information that governs the behavior of the ice and its interactions with the environment. Broadband scattering measurements of sea ice are presented beginning with ice-free conditions and through initial stages of growth in laboratory experiments for both congelation and frazil ice. With increased interest in drilling for hydrocarbon resources in the Arctic and the associated environmental concerns of an oil spill in ice-covered waters, improved methods for detection of crude oil both under or frozen within sea ice are needed. Acoustic scattering data are presented demonstrating how the scattering changes when crude oil is spilled beneath the ice.

Published by the Acoustical Society of America through the American Institute of Physics

 [DOI: 10.1121/1.4893927]
Received 7 Aug 2014; published 13 Aug 2014

INTRODUCTION

A significant portion of the world's estimated undiscovered oil is located in the Arctic [1]. The dramatic retreat of Arctic summer sea ice [2], has made increased shipping traffic and the development of these areas for hydrocarbon extraction increasingly likely. On-ice and airborne oil spill detection methods face technical and operational challenges in ice covered seas; there is a need to investigate other technologies for the application. At present, no studies have been published that apply broadband acoustic scattering techniques to sea ice or under-ice detection of oil spills. In order to identify oil under or within ice using acoustic techniques, it is necessary to understand acoustic scattering from sea ice.

The structure of sea ice during the early stages of growth is strongly dependent on the environmental conditions. Sea ice growth initiates through the formation of loose, flat dendritic crystals known as frazil ice. Under calm conditions, the frazil crystals will form an initial ice skim from which subsequent growth progresses vertically downward through congelation growth. Under turbulent conditions (e.g., surface waves), rapid freezing of loose frazil ice crystals occurs in the upper water. These frazil crystals will agglomerate and can, through repeated wave-induced collisions, consolidate into pancake ice [3]. Once the pancakes freeze together into a continuous ice cover, further thickening occurs through congelation ice growth. Congelation ice is characterized by columnar crystals with a so-called skeletal layer of parallel dendrites that extend into the seawater below. Between the dendrites, there are layers of seawater enriched with brine expelled from the ice during freezing. These complicated structures, present in the bottom centimeters of congelation ice, are referred to here as the skeletal layer. Even above this layer, the ice contains a complex interconnected brine network whose properties vary spatially and temporally with the salt content and temperature of the ice. The crystal size, crystal orientation, dendrite spacing, salinity, and brine and gas pocket distributions are all influenced by environmental conditions (e.g., currents), the ice growth rate, and method of ice formation [3].

The spatial scales associated with these different ice structures make high-frequency ($f > 10$ kHz) acoustic scattering techniques a viable potential tool for identification and characterization of the different ice structures, and consequently may reveal information about the interactions between the ice and the environment. High-frequency scattering from congelation ice has been measured in a limited number of previous studies using narrowband systems [4, 5]. These findings showed that roughness of the skeletal layer of congelation ice affects the echo statistics. Narrowband, multi-frequency methods have also been used to study frazil ice in rivers with the goal of inverting the results to estimate suspended frazil ice concentration [6, 7]. The authors are not aware of any studies applying broadband acoustic scattering techniques to congelation ice or frazil ice.

Here we present measurements of broadband backscatter from columnar and frazil ice grown in two separate laboratory experiments. In both cases, data were obtained during the initial stages of growth (≤ 2 cm of ice) until ice thickness was greater than or equal to 8 cm. Crude oil was then released in each tank. The measurements before and after the introduction of oil provide information about the acoustic scattering from both ice types and to illustrate how a crude oil spill changes the scattered signals.

METHODS: LABORATORY SETUP

The measurements of acoustic backscatter from congelation and frazil ice prior to and following the introduction of crude oil were performed from Dec. 12-20, 2013 at Hamburgische Schiffbau-Versuchsanstalt GmbH (Hamburg Ship Model Basin; HSVA) in Hamburg, Germany. Elevation views of the tanks used in these experiments are included in Fig. 1. The frazil tank was 1.5-m deep, 3-m wide, and 16-m long with a 3-m wavemaker at one end, and a "beach" at the other end to dissipate the surface waves. The frazil ice was formed in the wave tank by constantly running the wavemaker to produce waves (typically 0.1-m amplitude, 1.5 s period) while the room was maintained at temperature below -2°C. Under-ice observations were performed with instruments mounted to a trolley that could be moved along the bottom of the tank using wooden tracks and a pulley system. In addition to transducers for acoustic backscatter measurements, the trolley was also equipped with GoPro high definition cameras looking upwards at the water/ice interface and sideways at marks on the sides of the tank for determining the trolley's location. The frazil ice was grown to a thickness of roughly 8 cm before 10 L of oil were released under the frazil ice.

The columnar ice experiments were performed in a cylindrical tank (1.37-m deep, 1.4-m diameter) in a separate room maintained at a temperature of -18°C (Fig. 1a). Prior to the formation of ice, the salinity in the congelation tank was 32 PSU. On Dec. 16, when the acoustically inferred thickness of the ice was approximately 12 cm, 50 L of oil were released under the ice using a pipe frozen through the ice. In both experiments, the oil deployed was medium crude oil (API gravity = 30.75).

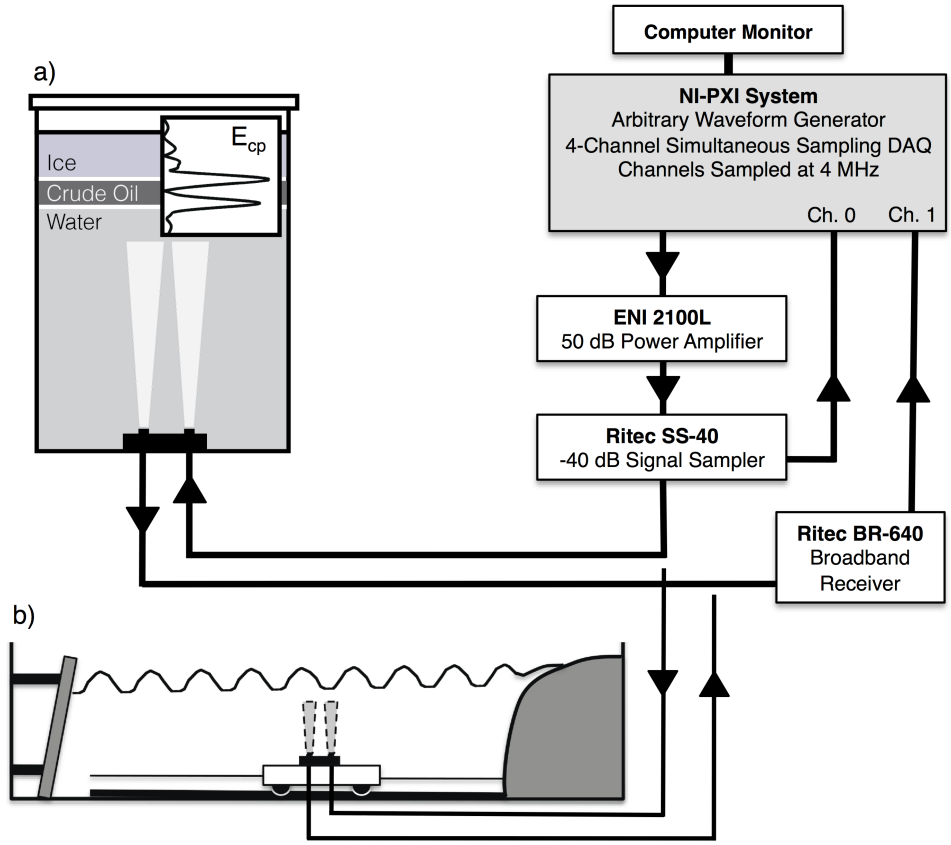

FIGURE 1. Illustration of the sampling scenarios (not to scale) in the congelation ice experiment (a), the frazil ice experiment (b), and a box diagram of the pulse-echo system. Simultaneous sampling of both experiments was not possible.

In both experiments, multiple pairs of transducers (closely spaced to approximate monostatic measurements) at different frequencies were used (Tab. 1): 350-565 kHz and 700-1050 kHz transducers in both experiments and a 200-300 kHz pair in the congelation ice experiments. In the frazil ice tank the trolley was positioned at the point of interest and a single transducer pair sampled the backscatter at the maximum possible sampling rate. The frazil ice data presented in this document were sampled at 5.3 Hz for 200 pings for a sampling period of approximately 38 s (24 wave periods). Identical sampling with the second transducer pair immediately followed the samples with the first pair.

Two types of sampling were performed in the congelation ice tank. First, at least once per day sampling was performed using all of the transducer pairs. Each pair sampled at 1 Hz for a minimum of 30 pings. Over these time scales no variations in backscatter attributed to the ice were observed and the data averages of the pulse compressed data (see following section) was performed to reduce noise. Second, overnight operation of the system was used to produce a time series of backscatter during ice growth. The data presented here were sampled every 90 s using a 1 MHz transducer pair and the analysis was performed on the individual pings (no averaging).

METHODS: DATA ACQUISITION AND PROCESSING

An elevation view of the configuration for the congelation ice experiment and a description of the pulse-echo system hardware used for both experiments is described in Fig. 1. The same pulse-echo hardware was used in the frazil ice experiment. Data acquisition was performed with a custom LabView script. The transmit and received signals were sampled at 4 MHz. All transmitted signals were 250 μs linearly modulated chirps. The transducer pairs were calibrated after allowing surface disturbances in the tank to settle overnight and using the smooth, pressure release surface as an ideal reflector.

TABLE 1. Transducer parameters for both experiments. The footprints are calculated at a range of r_{scat} =0.7 m for the frazil ice experiment and r_{scat} =0.85 m for the congelation ice experiment.

Transducer parameter	Congelation Ice Tank			Frazil Ice Tank	
Frequency range (kHz)	200-300	350-565	700-1050	350-565	700-1050
Center frequency (kHz)	250	500	1000	500	1000
Wavelength, λ, (mm)	5.7	2.9	1.4	2.9	1.4
Transducer diameter, D (cm)	2.54	1.91	2.54	2.54	1.91
Full beamwidth, θ ($^\circ$ at - 3 dB)	13.4	8.8	3.4	6.6	4.4
Far field, D^2/λ (cm)	2.8	3.2	11.2	5.6	6.3
Fresnel radius, $r_{scat}\tan(\frac{\theta}{2})$ (cm)	4.9	3.5	2.5	3.2	2.3
Footprint radius, $r_{scat}\tan(\frac{\theta}{2})$ (cm)	11.3	7.5	3.8	5.3	3.8
Bandwidth (B) (kHz)	100	215	350	215	350
Spatial resolution (cm) - pulse length ($\frac{1}{2}c_{\mathrm{w}}T$)	18	18	18	18	18
Spatial resolution (cm) - pulse compression ($\frac{c_{\mathrm{w}}}{2B}$)	0.7	0.3	0.2	0.3	0.2

Pulse-compression techniques [8, 9], which result in improved range resolution and signal-to-noise ratios in comparison to narrowband methods, were used to analyze the scattered signals in the temporal domain. These results are presented in terms of the pulse compressed (CP) output, E_{CP}. The range to the first interface (water/ice or water/oil) is given by: $r = \frac{c_{\mathrm{w}}}{2}t_1$, where c_{w} is the sound speed of the water (c_{w} =1440 m/s) and t_1 is the delay time to the first peak in E_{CP}. In the congelation ice experiment, the ice thickness was inferred using the change in time delay from the calibration data (i.e., the water/air interface). Once introduced under congelation ice, the buoyant oil forms a layer under the ice and E_{CP} contains two peaks, which is consistent with backscatter from two interfaces. The thickness of the oil is given by: $h_{\mathrm{oil}} = (c_{\mathrm{oil}}/2)\,|t_2 - t_1|$, where c_{oil} is the sound speed of the oil, and t_1 and t_2 are the time delays of the peaks in E_{CP} that are attributed to the water/oil and oil/ice interfaces (e.g., E_{CP} in Fig.1a).

The frequency spectra of the received scattered signals are presented in the form used by Lavery and Ross (2007) [10, Eq. 1]. That is,

$$P_{ratio}(\omega) = \frac{P_{scat}(\omega)}{P_{inc}(\omega)} = G(\omega)\frac{V^R(\omega)}{V^R_{cal}(\omega)}\frac{r_{scat}}{r_{cal}}, \tag{1}$$

where ω is the angular frequency, P_{scat} is the amplitude of the scattered pressure, P_{inc} is the amplitude of the incident pressure at the scattering interface, r_{cal} is the range to the surface during calibration, and r_{scat} is the range to the scattering interface. $V^R(\omega)$ and $V^R_{cal}(\omega)$ are the absolute values of the Fourier transforms of the received voltage time series and the received calibration voltage time series, respectively. $G(\omega) = V^T_{cal}(\omega)/V^T(\omega)$ is the ratio of the absolute value of the Fourier transform of the transmit voltage calibration time series to the absolute value of the transmit voltage time series. All Fourier transforms use 2048 data points, which is roughly twice the length of the transmitted signal and captures the full length of the scattered signals. This formulation accounts for the range dependence of the incident pressure but not the range dependence of the scattered pressure. For an acoustically smooth interface, this formulation for P_{ratio} is equivalent to a reflection coefficient. The attenuation in water is neglected due to the short ranges ($r_{scat} < 1$m).

RESULTS: FRAZIL ICE AND OIL

As a surface wave passes, buoyant frazil crystals are displaced vertically with the ice/air interface. The envelopes of the CP output during the frazil experiments show a well-defined water/ice interface above which peaks in the CP output decrease in amplitude (Fig. 2a). These patterns are consistent with volume scattering and high attenuation rates in the frazil ice. At the time the measurements in Fig. 2 were obtained there was only 8 cm of frazil ice [11] but there is no clear signal from the ice/air interface. Other than the vertical displacement of the water/ice interface there are no clear relationships between the phase of the surface wave and the received signals analyzed in either the temporal (Fig. 2a) or frequency (Fig. 2b) domains. This result is surprising given the expected compression and expansion of the frazil ice in the peaks and troughs of the passing waves could locally modulate the frazil crystal concentration. Little or no signal from frazil crystals suspended in the water column due to downward turbulent mixing was observed. The lack of observations consistent with either of these processes is attributed to insufficient wave energy in the experiments to drive these processes. Due to the lack of surface wave phase dependence, the frequency-dependent backscatter is

averaged over many wave periods (Fig. 2c). For the frazil ice P_{ratio} is proportional to f^2, ranging from -14 dB to -5 dB. Thus, P^2_{ratio} is proportional to f^4, as is expected for scattering in the Rayleigh regime.

Acoustic backscatter and video measurements were obtained before, during, and after the oil release. The oil is poured into a funnel attached to a hose running under the ice to the bottom of the tank. The oil flow, driven by hydrostatic pressure, becomes unstable and breaks into drops that rise to the surface as has been reported previously [12]. When the rising droplets reach the water/frazil ice interface they temporarily pool under the frazil ice layer changing the observed backscatter from the interface (Fig.3). As successive waves pass, the buoyant oil rises through the frazil layer to the ice/air interface where it spreads horizontally. As the oil rises through the layer the backscattered signal from the oil diminishes.

Images of the oil release and spreading within the frazil ice and post-experiment ice cores are available in Figs. 2-6 of *Wilkinson et al.* (2014) [11]. For a brief period ($<$ 2 min.) following the introduction of the oil the amplitude of E_{CP} increased by more than a factor of three while the width of E_{CP} decreased and contained most of the energy in a single peak rather distributed through the frazil layer like the envelopes in Fig. 2a. Example signals approximately one minute before, during, and one minute after the oil release are included in Fig.3.

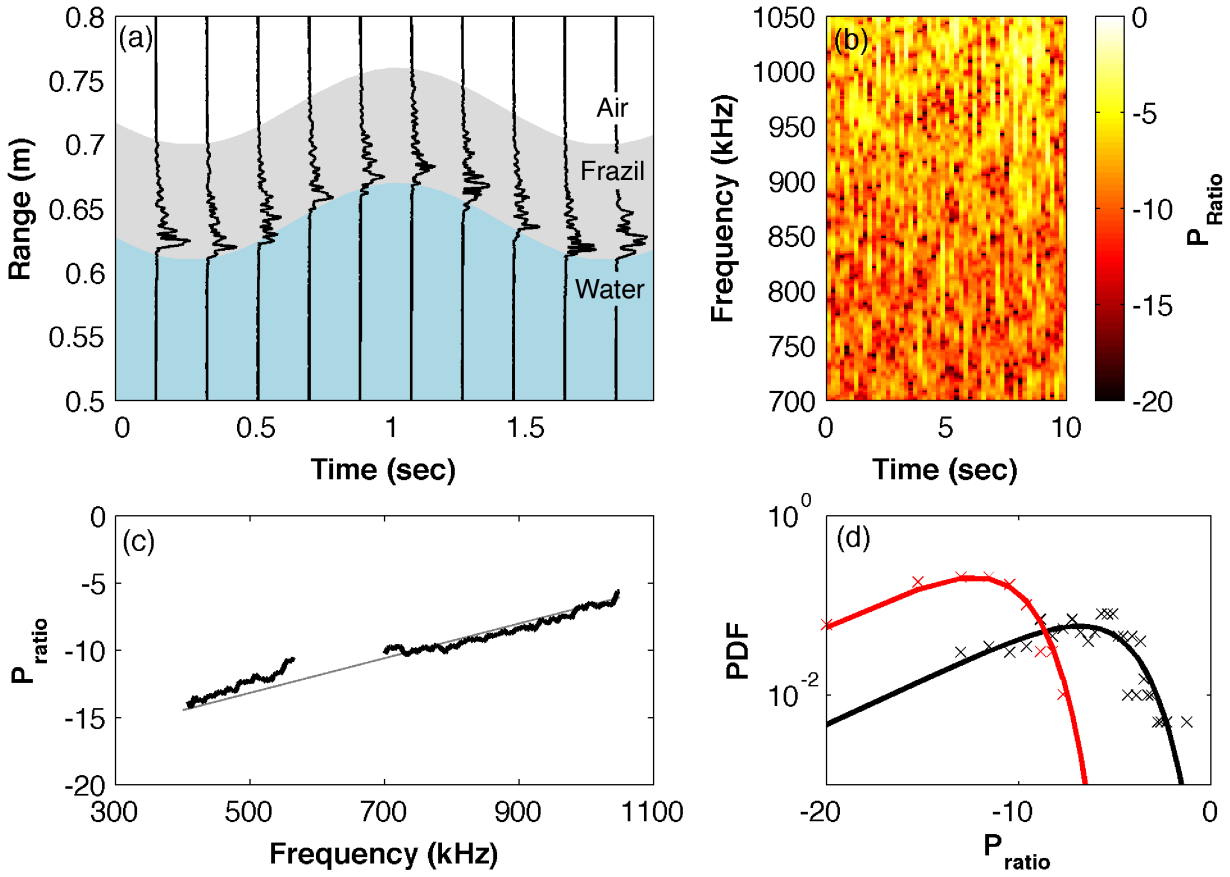

FIGURE 2. Acoustic backscatter data from frazil ice prior to the introduction of oil. (a) E_{CP} with approximately 8 cm of frazil ice. The ping rate is 5.3 Hz. (b) Spectrogram of P_{ratio} for frazil ice. (c) P_{ratio} averaged over 200 pings (black) and a line showing a f^2 dependence (gray). (d) Echo statistics for the 500 kHz (red x's) and 1000 kHz (black x's) data and the Rayleigh PDFs for the mean P_{ratio} in (c).

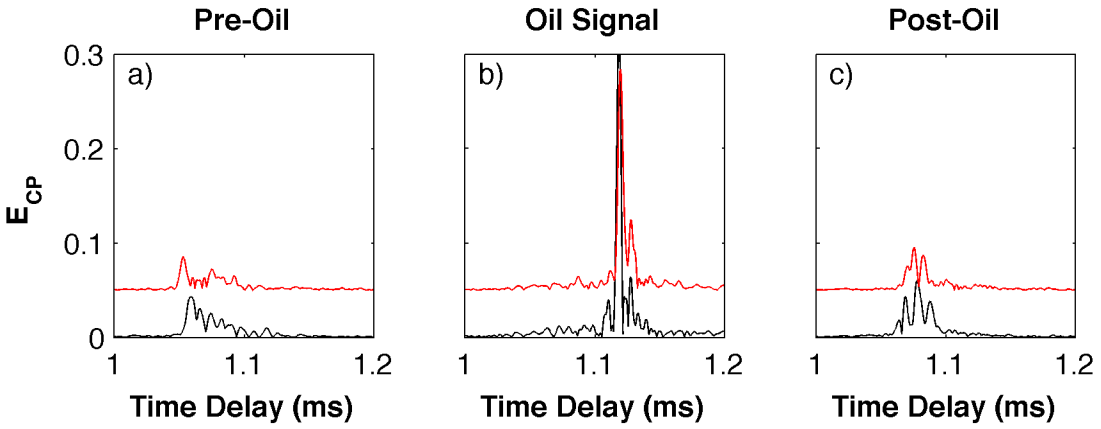

FIGURE 3. Examples of backscattered signals before, during, and after the the introduction of oil in the frazil experiment. All signals were associated with wave troughs so changes in the time delay are attributed to the presence of oil. (a) Frazil measurements 60 seconds before the clear signal of oil. (b) Signals attributed to the oil. (c) Measurements 60 seconds after the clear signals of oil.

RESULTS: CONGELATION ICE AND OIL

The backscatter measurements under congelation ice, prior to the introduction of oil, are influenced entirely by the structure of the ice in the skeletal layer. Fig. 4a includes CP envelopes for the calibration signals (water/air interface) and for the water/ice interface, for all three transducers. The signals scattered from the water/ice interface increase in complexity with frequency, which is likely a result of both the spatial/temporal resolution of the signals increasing with frequency due to the increasing bandwidth and the roughness of the ice increasing relative to the acoustic wavelengths.

During overnight periods, a single transmit/receive pair of 1 MHz transducers sampled at regular intervals to monitor changes in backscatter during ice growth. Fig. 5 includes a set of CP envelopes obtained during a 10-hour period beginning on Dec. 14. The envelopes show elevated backscatter within the bottom 5 cm of the ice. Notably, typical structural features in the envelopes do not persist for periods longer than two hours. Further inspection of the evolution of the envelopes in time reveals oscillations on time scales significantly shorter than those associated with ice growth. For example, in Fig. 5 the acoustically inferred distance to the bottom of the ice using a sound speed of 1440 m/s changes by less than 1 cm during the period. During the same period peaks in the envelopes appear and disappear numerous times. Not only do these results indicate that changes occur in the amplitude of the returns on time scales greater than a few hours, they also oscillate on time scales less than one hour. The source of these backscatter variations is uncertain, as independent observations of possible structural or compositional small-scale variations in the skeletal ice layer were not made (and, indeed, are very challenging to make). Changes in the internal pore structure of sea ice occur during growth [14] but the timescales of these changes are likely to be greater than the observed changes in scattering. However, previous studies demonstrated that cyclical temperature changes occur within a few centimeters of the ice/water interface as convection occurs and brine is rejected from the growing ice [15]. Our hypothesis is that the changes in backscatter are driven by density and temperature fluctuations associated with convention or brine rejection.

Despite the complexity at higher frequencies, two interfaces can be identified in the envelopes once the oil is introduced (Fig. 4a). The oil thickness is acoustically inferred from the 200-300 kHz temporal data to be approximately 4 cm thick assuming a sound speed in oil of 1475 m/s [13]. Similar inferences can be made from the higher frequency transducers, but the additional complexity of the signals results in more ambiguity in identifying the closely spaced interfaces. The spectra of the backscattered signals are shown in Figs. 4b and 4c for pre- and post-oil measurements. In pre-oil measurements the spectra of the backscattered signals indicate some structure that suggests the interface is not acoustically smooth. In the measurements with oil, the spectra exhibit structure that is consistent with reflections from a layered medium. More specifically, there is a pattern of peaks and nulls that is consistent with constructive and destructive interference from two interfaces.

CONCLUSIONS

In frazil ice, the observed backscatter is consistent with expectations for volume scattering from a number of small, loose ice crystals while in congelation ice the backscatter is attributed to the complex skeletal layer at the ice/water interface. In the latter case, temporal changes on time scales of several hours were observed that may be related to compositional changes caused by brine dynamics at and within the skeletal layer of the ice. This suggests that broadband acoustic methods may be useful for non-destructive investigations of sea ice growth processes

While high-frequency, broadband acoustic backscatter can be used to distinguish oil from different laboratory-grown ice morphologies, the complex nature of the scattering from differing ice types, including temporal changes that may reflect acoustic signatures at different stages of ice growth, is a complicating factor. Under congelation ice, the layered nature of the oil-ice system facilitates the identification of oil. For ice types like frazil where the oil can percolate into the ice cover, well-defined layers were not observed and changes in scattering were only observed during the spill, suggesting that other methods of oil detection are likely to be more effective.

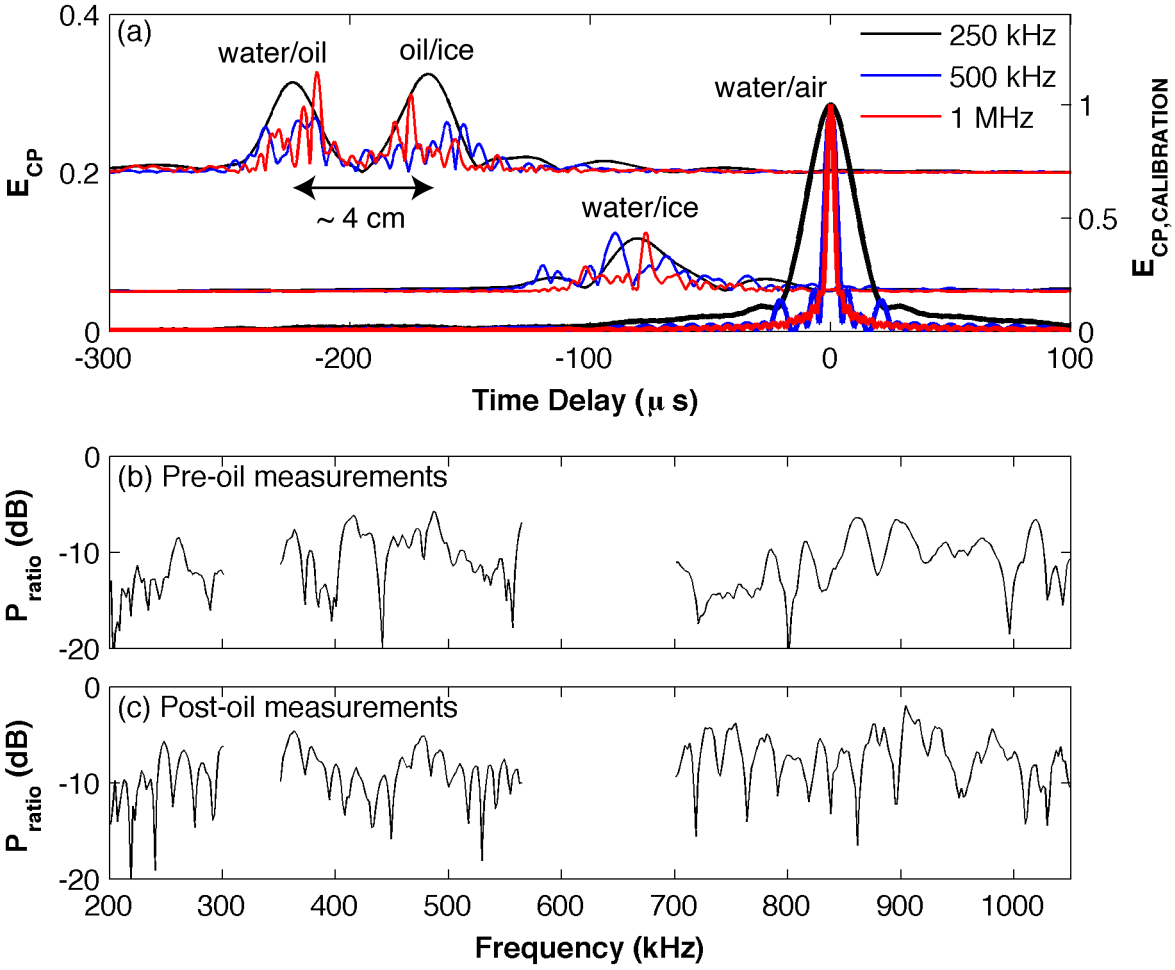

FIGURE 4. (a) Three sets of envelopes show the temporal data at different time during the experiments. From bottom to top the envelopes correspond to the calibration data with the water/air interface, the water/ice interface after roughly 6 cm ice growth, and the water/oil and oil/ice interfaces. Assuming an oil sound speed of 1475 m/s, the acoustically inferred oil thickness is approximately 4 cm. In general, the increasingly complex envelopes at higher frequency make it more difficult to identify interfaces. (b) Frequency-spectrum of scattering from the water/ice interface from 200-1050 kHz. (c) Frequency-spectrum of scattering from the water/oil and oil/ice interfaces (black lines) from 200-1050 kHz. The patterns of peaks and nulls in the spectra are consistent with scattering from two interfaces.

ACKNOWLEDGMENTS

The authors thank the staff at HSVA, especially Karl Ulrich-Evers, for their technical support. Dale Chayes and Chris Calihan also provided support during the experiment. Funding for the work was provided by the U.S. Bureau of Safety and Environmental Enforcement contract number E12PC00053. Christopher Bassett was supported by the WHOI Postdoctoral Scholar Program with funding provided by the United States Geological Survey.

REFERENCES

1. D.L. Gautier, K.J. Bird, R.R. Charpentier, A. Grantz, D.W. Houseknecht, T.R. Klett, T.E. Moore, J.K. Pitman, C.J. Schenk, J.H. Schuenemeyer, K. Sørensen, M.E. Tennyson, Z.C. Valin, and C.J. Wandrey. Assessment of undiscovered oil and gas in the Arctic. *Science*, 324(5931):1175Ð1179, 2009.
2. D. J. Cavalieri and C. L. Parkinson. Arctic sea ice variability and trends, 1979Ð2010. *Cryosphere*, 6:881Ð889, 2012.
3. W. F. Weeks. *On Sea Ice*. University of Alaska , Fairbanks, Alaska, 2010.
4. T. K. Stanton, K. C. Jezek, and A. J. Gow. Acoustical reflection and scattering from the underside of laboratory grown sea ice: Measurements and predictions. *J. Acoust. Soc. Am.*, 80(5): 1486–1494, 1986.
5. K. C. Jezek, T. K. Stanton, A. J. Gow, and M. A. Lange. Influence of environmental conditions on acoustical properties of sea ice. *J. Acoust. Soc. Am.*, 88(4): 1903–1912, 1990.
6. J.R. Marko and M. Jasek. Sonar detection and measurement of ice in a freezing river II: Observations and results on frazil ice. *Cold Reg. Sci. Technol.*, 63: 135–153, 1960.
7. M. Richard, B. Morse, S.F., and J. Emond. Quantifying suspended frazil ice using multi-frequency underwater acoustic devices. *River Res. Appl.*, 27: 1106–1117, 1960.
8. G. L. Turin. An introduction to matched filters. *IRE Trans. Inf. Theory*, 6(3): 311–329, 1960.
9. D. Chu and T. K. Stanton. Application of pulse compression techniques to broadband acoustic scattering by live individual zooplankton. *J. Acoust. Soc. Am.*, 104(1): 39–55, 1998.
10. A. C. Lavery and T. Ross. Acoustic scattering from double-diffusive microstructure. *J. Acoust. Soc. Am.*, 122(3): 1449–1462, 2007.
11. J. Wilkinson, T. Maksym, C. Bassett, A.C. Lavery, H. Singh, D. Chayes, P. Elosegui, P. Wadhams, K. Ulrich-Evers, and P. Jochmann. Experiments on the detection and movement of oil spilled under sea ice. *Proc. HYDRALAB IV Joint User Mtg.*, Lisbon, Portugal. July 2-4, 2014.
12. NORCOR Engineering and Research Ltd. The interaction of crude oil with arctic sea ice. Beaufort Sea Technical Report, no. 27. Technical report, Beaufort Sea Project, Department of the Environment, Victoria, 1975.
13. M. Batzle and Z. Wang. Seismic properties of pore fluids. *Geophysics*, 57(11): 1396–1408, 1992.
14. D. J. Pringle, J. E. Miner, H. Eicken, and K. M. Golden. Pore space percolation in sea ice single crystals. *J. Geophys. Res.*, 114(C12017): 1–14, 2009.
15. R.A. Lake and E.L. Lewis. Salt rejection by sea ice during growth. *J. Geophys. Res.*, 75(3): 583–597, 1970.

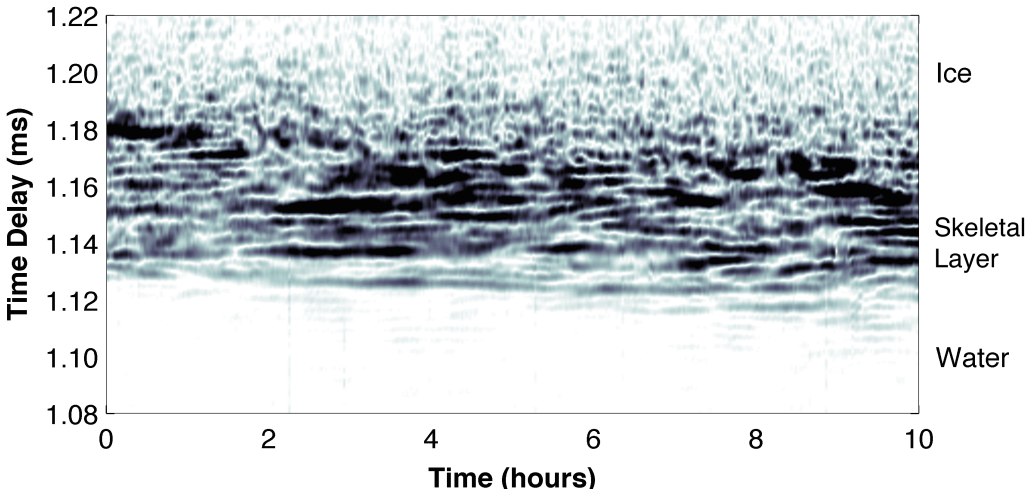

FIGURE 5. Time series E_{CP} during from Dec. 14 using a 1 MHz transducer pair. Assuming a sound speed of 1440 m/s (water), the scale of the y-axis is approximately 10 cm. The development and subsequent decay of structures in E_{CP} occurs over periods less than 2 hours.